Original Article

Early rectal neoplasm in dual-layer spectral detector computed tomography: dual-layer spectral computed tomography (CT) images improve tumor detection and staging

Xuelin Pan[1#], Zhihan Wu[2,3#^], Jin Zhao[1], Xinyi Zhang[1], Xiaodi Zhang[1], Li Tang[2,3], Jinlin Yang[2,3*], Kai Deng[2,3*^]

[1]Department of Radiology, West China Hospital, Sichuan University, Chengdu, China; [2]Department of Gastroenterology and Hepatology, West China Hospital, Sichuan University, Chengdu, China; [3]Sichuan University-University of Oxford Huaxi Joint Center for Gastrointestinal Cancer, Department of Gastroenterology & Hepatology, West China Hospital, Sichuan University, Chengdu, China

Contributions: (I) Conception and design: X Pan, K Deng; (II) Administrative support: X Pan, K Deng, J Yang; (III) Provision of study materials or patients: X Pan, Z Wu; (IV) Collection and assembly of data: X Pan, Z Wu; (V) Data analysis and interpretation: J Zhao, Xinyi Zhang, Xiaodi Zhang, L Tang; (VI) Manuscript writing: All authors; (VII) Final approval of manuscript: All authors.

[#]These authors contributed equally to this work as co-first authors.

[*]These authors contributed equally to this work as corresponding authors.

Correspondence to: Jinlin Yang, MD; Kai Deng, MD. Department of Gastroenterology and Hepatology, West China Hospital, Sichuan University, 37 Guoxue Lane, Chengdu 610041, China; Sichuan University-University of Oxford Huaxi Joint Center for Gastrointestinal Cancer, Department of Gastroenterology & Hepatology, West China Hospital, Sichuan University, Chengdu, China. Email: yangjinlin@wchscu.cn; dengkai@wchscu.cn.

Background: Early rectal neoplasms can be treated endoscopically with good prognosis, yet usually present with unspecific or an absence of signs and symptoms and are detected largely by invasive endoscopy with less compliance to screening. The purpose of this cross-sectional study was to explore the diagnostic value of dual-layer spectral detector computed tomography (DSCT) imaging for early rectal neoplasm.

Methods: Patients who underwent DSCT for evaluation of rectal lesion or routine examination between September 2022 to September 2023 at West China Hospital were prospectively included and identified as group A (control, n=76), group B (rectal advanced adenomas and ≤T1 rectal cancer, n=59), and group C (≥T2 staging rectal cancer, n=74). Lesion visualization was graded to assess image quality. Spectral quantitative measurement, such as Hounsfield unit $(HU)_{40\ keV}$, $HU_{70\ keV}$, iodine concentration (IC), effective atomic number (Zeff), and the slope of spectral curve (λ), was analyzed and compared. Receiver operating characteristic (ROC) curves were generated to evaluate the diagnostic efficacy of spectral parameters. A comparison of ROC curves was applied to test the significance of differences between the area under the curves (AUCs).

Results: Compared to poly-energetic images (PEIs), the multiple parameters from DSCT were of greater capability to recognize rectal lesions. There were significant differences in $HU_{40\ keV}$ (208.01±43.60 *vs.* 255.53±45.16), $HU_{70\ keV}$ (87.06±18.55 *vs.* 100.78±18.26), IC [1.91 (1.71, 2.28) *vs.* 2.58±0.49], Zeff [8.33 (8.25, 8.50) *vs.* 8.61±0.20], and λ [3.80 (3.41, 4.52) *vs.* 5.16±1.00] between the early neoplastic lesions in rectum and the advanced rectal cancer (P<0.001). Significant correlations were found between the DSCT parameters and tumor staging (P<0.001). Furthermore, the AUCs of IC, Zeff, λ, and HU_{PEI} were all above 0.90 for early rectal neoplasm detection, with additional capability of discriminating early rectal neoplasm from advanced

^ ORCID: Kai Deng, 0000-0002-0096-5211; Zhihan Wu, 0000-0002-6158-3612.

rectal cancer.

Conclusions: DSCT improved tumor conspicuity and the detection of the early rectal neoplastic lesion, suggesting that it is a promising screening tool in clinical practice.

Keywords: Dual-layer spectral detector computed tomography (DSCT); early neoplasm; rectum; detection

Submitted Apr 23, 2024. Accepted for publication Aug 22, 2024. Published online Oct 28, 2024.
doi: 10.21037/qims-24-769
View this article at: https://dx.doi.org/10.21037/qims-24-769

Introduction

As the third most common cancer worldwide and the second leading cause of cancer death (1), colorectal cancer (CRC) has made up a large proportion of the mortality rate and healthcare costs. Approximately 15–30% of CRC patients present with synchronous metastases, and 20–50% of patients with initially localized CRC will develop metastases (2), which usually leads to worse outcomes despite surgical resection or chemoradiotherapy. Thus, early detection is essential for accurate selection of patients with early neoplastic lesions in the rectum.

Early rectal neoplasms usually present with unspecific or an absence of signs and symptoms; detection is largely dependent on invasive endoscopic examination, which is associated with reduced patient compliance (3). There is an urgent need for a non-invasive screening tool. Biomarker detection is a patient-friendly approach which improves patient compliance to CRC screening, although the method currently has low specificity and accuracy (4,5). Despite its high spatial resolution, computed tomography (CT) has yielded a high rate of missed superficial and minimal early neoplasms, due to the rather thin and tortuous intestinal wall, usually combined with motion artifacts and the interference of content (6). Technological advancements have improved the opportunity to detect cancer early, increasing the prospects for treatment and curative intent. Dual-layer spectral detector CT (DSCT) has emerged as a novel and promising imaging modality, which uses two detector layers and an X-ray tube. The two measurement projection data in DSCT scanning are perfectly matched in temporal and spatial co-registration. Another benefit of DSCT is that the energy spectrum scanning is realized simultaneously as conventional scanning without any additional steps or contrast media (7). Recent studies have demonstrated the ability of DSCT to improve image quality, diagnostic accuracy of histological type, staging, and risk stratification with its virtual monochromatic and quantitative material decomposition images (8-11), but data showing its ability to detect early rectal neoplasms are scarce. The purpose of this study was to evaluate the diagnostic efficacy of DSCT in the detection of early rectal neoplasm. We present this article in accordance with the STROBE reporting checklist (available at https://qims.amegroups.com/article/view/10.21037/qims-24-769/rc).

Methods

Patients

The study was conducted in accordance with the Declaration of Helsinki (as revised in 2013). This prospective study was approved by West China Hospital Institutional Review Board (No. 2024-378) and informed consent was provided by all individual participants. During September 2022 to September 2023, patients at West China Hospital who were initially diagnosed with untreated neoplastic lesions in the rectum (advanced adenomas or rectal cancer) confirmed by pathological or clinical information were suggested to receive intravenous contrast-enhanced abdominal DSCT scanning for further preoperative evaluation. The exclusion criteria included history of preoperative therapy, such as endoscopic mucosal resection, endoscopic submucosal dissection, radiotherapy, or chemotherapy, metal abdominal implants, severe artifacts on CT images, and incomplete clinical data. Stratified by postoperative pathology, patients with rectal advanced adenomas and ≤T1 rectal cancer were labelled as group B (endoscopically-amenable group), whereas patients with ≥T2 rectal cancer were labelled as group C (advanced rectal cancer group). At the same time, patients at the West China Hospital without any rectal malignancy, as confirmed by endoscopy and follow-up, who underwent abdominal DSCT scanning for examination were also recruited as controls, labelled as group A, the benign group; these patients are also adhered to the exclusion criteria. All the

included patients completed the entire CT scanning and there were no artifacts in their images.

Imaging protocol

CT scans were performed on a Spectral CT 7500 (Philips Healthcare, Best, The Netherlands) scanner with no rectal contrast or distension applied. The helical scan range was determined by a scout scan, and included the entire abdomen from the diaphragms to the pubic symphysis. Following the scout scan, CT scan parameters were as follows: tube voltage, 120 kV; tube current, automated exposure modulation; detection collimation, 128×0.625 mm; rotation time, 0.4 s; and helical pitch, 1.1. Patients were then injected with a total dose of 70–100 mL (1.0–1.2 mL per kilogram of body weight) of nonionic iodinated contrast material (Iopamidol 370 mg/mL; Bracco Sine Phamaceutical Co., Ltd., Shanghai, China) at a rate of 2.5–3 mL/s using a power injector. Bolus tracking was utilized with the region of interest (ROI) placed in the aorta, and image acquisition started 7 seconds after the signal attenuation reached the predefined threshold of 100 Hounsfield units (HU) for the arterial phase. A 30-second delay was utilized as the venous phase. Contrast-enhanced CT scans of the pelvic area were performed in the venous phase. All the images were reconstructed with 2 mm slice thickness and 2 mm interval for axial images, with iDose^4 algorithm for poly-energetic images (PEIs) and spectral reconstruction (level 4) for spectral images, respectively.

Image generation

The PEIs and quantitative spectral analysis were performed by IntelliSpace Portal software (Version 12.0; Philips Healthcare). The spectral-based image data were post-processed to generate different image types, including iodine concentration (IC) images (iodine map), effective atomic number (Zeff) images, and virtual mono-energetic images (40 and 70 keV).

Objective image analysis

All the images were shuffled and analyzed independently by two radiologists with more than 10 years of experience in abdominal radiology (X.P and J.Z.), who were blinded to the clinical and pathological information.

First, the 40 keV images were evaluated to localize and identify tumor. Second, a freehand ROI was placed at the 40 keV images on the normal bowel wall (group A, $B_{\text{bowel wall}}$ and $C_{\text{bowel wall}}$) or the lesion (group B_{tumor} and C_{tumor}, diameter of about one to two-thirds of the lesion size), avoiding regions of necrosis, calcification, and artifacts caused by the gas and liquid interface, as the ROI then would be copied to other images. Image slices containing the maximum cross-section for the tumor and the slice above and below were chosen for measurement. The average values of all the ROIs were calculated to minimize the measurement bias. Third, measurements were performed on both the lesion and the normal bowel wall, recording CT values at 40 keV, 70 keV and PEI image, IC value at iodine map, and Zeff value at Zeff images (*Figure 1*).

The slope of the spectral curve (λ) (8) and tumor contrast (12) were calculated according to the following formulas:

$$\lambda = \left(HU_{40\,\text{keV}} - HU_{70\,\text{keV}}\right)/30 \quad [1]$$

$$\text{Tumor contrast} = HU_{tumor} - HU_{bowel\ wall} \quad [2]$$

Subjective image analysis

The aforementioned two radiologists reviewed the virtual monochromatic images and PEIs. A 3-point Likert scale was used to rate rectal neoplasm conspicuity: Grade 1: not visualized; Grade 2: nondiagnostic due to blurring lesions; Grade 3: clearly and entirely visualized) (*Figure 2*) (12).

Statistical analysis

Statistical analysis was performed using the software SPSS 27.0 (IBM Corp., Armonk, NY, USA), GraphPad Prism version 8.0.2 (GraphPad Software, Inc, Boston, MA, USA), and MedCalc® Statistical Software version 19.2.6 (MedCalc Software Ltd., Ostend, Belgium).

The kappa coefficient (κ) was used to measure the inter-reader agreement of the tumor conspicuity (κ=0.81–1.00 excellent; 0.61–0.80 substantial; 0.41–0.60 moderate; 0.21–0.40 fair; 0.00–0.20 poor) (13-15).

Data distribution was assessed by the Shapiro-Wilk test. Continuous variables were presented as mean ± standard deviation (SD) or median [interquartile range (IQR)]. Tumor contrast was compared by paired *t*-test or Wilcoxon test. The differences in the average values of $HU_{40\,\text{keV}}$, $HU_{70\,\text{keV}}$, HU_{PEI}, λ, IC, and Zeff among groups were statistically analyzed using independent/paired *t*-test, Mann-Whitney U test, or Wilcoxon test. The relationship

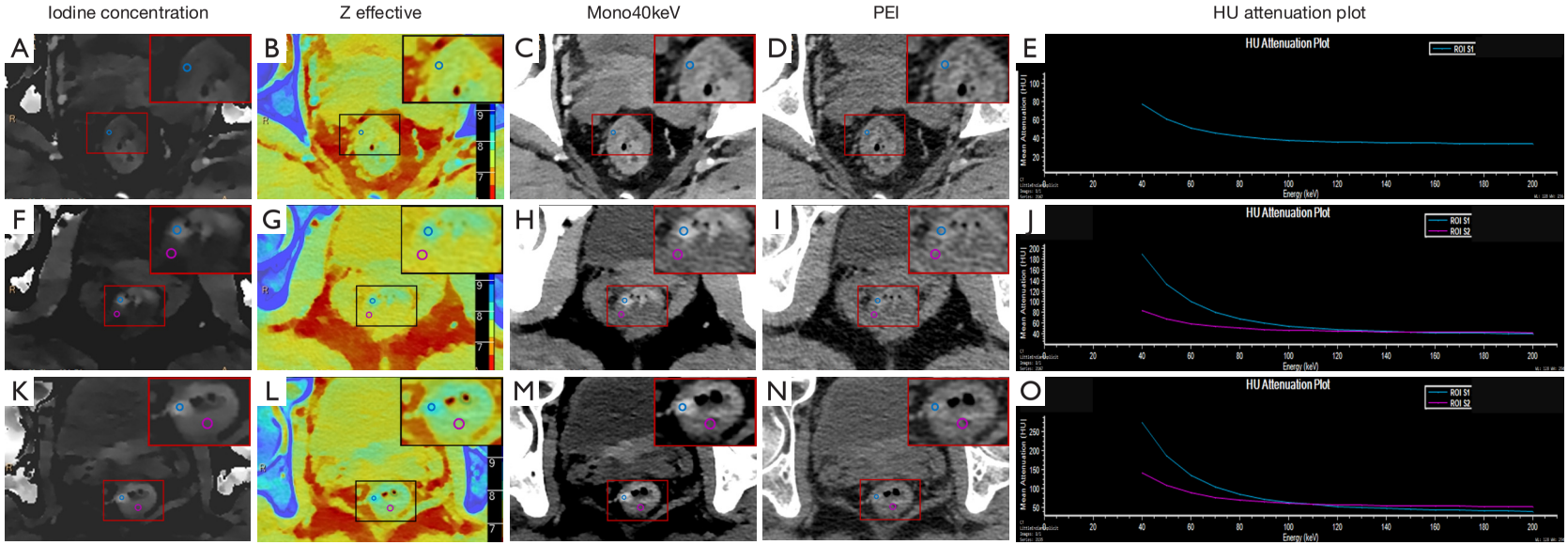

Figure 1 DSCT images of three groups. (A-D) Group A. ROIs were placed on the iodine-based decomposition images (A), and copied to the (B) Zeff, (C) mono40keV, and (D) PEIs. The same for the group B (F-I) and group C (K-N) (blue for the lesion, purple for the control). The area in the box was enlarged on the upper right corner. Spectral HU curves in (E) group A, (J) group B (blue for the lesion, purple for the control), and (O) group C (blue for the lesion, purple for the control). PEI, poly-energetic image; HU, Hounsfield unit; DSCT, dual-layer spectral detector computed tomography; ROIs, regions of interest; Mono40keV, mono-energetic images of 40 keV.

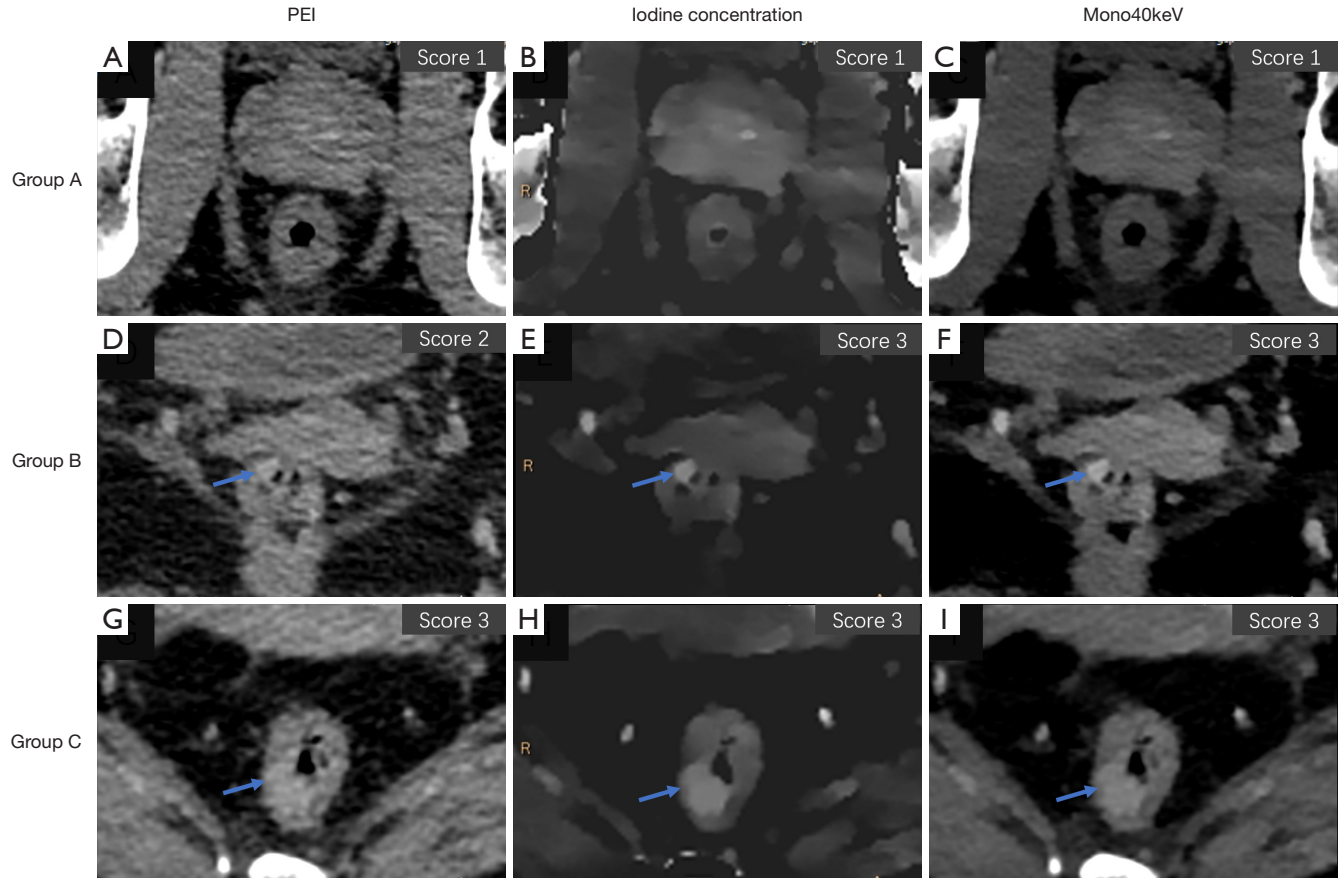

Figure 2 Likert scale for rectal neoplasm visualization. (A,D,G) PEIs of three groups scored (A) 1, (D) 2, (G) 3, respectively. (B,E,H) Iodine-based decomposition images of three groups scored (B) 1, (E) 3, (H) 3, respectively. (C,F,I) Mono40keV images of three groups scored (C) 1, (F) 3, (I) 3, respectively. Lesion (blue arrows). PEI, poly-energetic image; Mono40keV, mono-energetic images of 40 keV.

of lesion staging and spectral parameters was analyzed using Kendall's tau. Receiver operating characteristic (ROC) curves were calculated to evaluate the diagnostic values of each parameter in lesion visualization and discriminating advanced and early rectal neoplasms. A comparison of ROC curves was applied to test the significance of differences between the area under the curves (AUCs). Statistical significance was defined as $P<0.05$ (2-sided).

Results

Patients

Finally, a total of 209 patients who underwent DSCT from September 2022 to September 2023 were prospectively enrolled with a mean age of 59.0 (53.0, 68.0) years and 47.8% men (n=100), with 76 patients in group A, 59 in group B, and 74 in group C. There were 77 lesions in group B and 74 lesions in group C (*Figure 3*).

Lesion detection

The two radiologists showed moderate agreement in regard to the rectal neoplasm visualization grading (κ=0.509). Tumor conspicuity was rated best on mono40keV and IC images compared to that of PEI regardless of grouping, whereas no significant difference was found between mono40keV images and IC images (*Figure 4A-4F*, *Table 1*). Tumor contrast was higher in mono40keV images than the PEIs [Group B+C, 121.50 (98.30, 158.50) *vs.* 44.53±23.41, $P<0.001$; Group B, 104.90 (90.55, 134.40) *vs.* 43.02±22.45, $P<0.001$; Group C, 148.04±46.09 *vs.* 46.11±24.42, $P<0.001$], whereas that of the mono70keV images was not statistically significant in Group B+C (45.09±20.71 *vs.* 44.53±23.41,

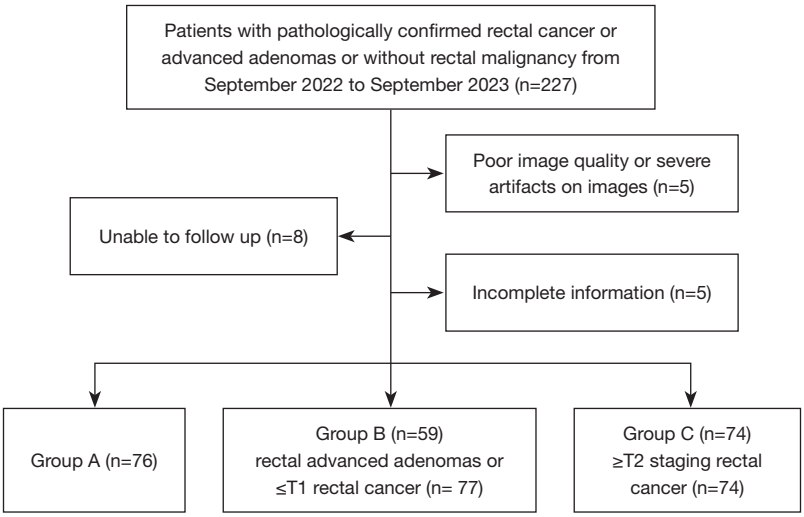

Figure 3 Flowchart of patient selection. Group A, the benign group; Group B, the endoscopically-amenable group; Group C, the advanced rectal cancer group.

P=0.385) and Group B (42.29±20.36 *vs.* 43.02±22.45, P=0.415) (*Figure 4G-4I*).

DSCT findings of different groups

The $HU_{40\ keV}$, $HU_{70\ keV}$, IC, Zeff, and λ were significantly higher for the rectal lesion than the benign bowel wall (P<0.001), and also for the advanced rectal cancer than the early rectal neoplasms (P<0.001), whereas most parameters showed no significant differences among benign groups (P>0.05, *Table 2*, *Figure 5*). As for HU_{PEI}, there were statistically significant differences between $B_{bowel\ wall}$ and B_{tumor} (44.50±13.99 *vs.* 86.68±19.87, P<0.001), $C_{bowel\ wall}$ and C_{tumor} (53.70±13.64 *vs.* 99.73±20.53, P<0.001), whereas no significant difference between B_{tumor} and C_{tumor} (86.68±19.87 *vs.* 99.73±20.53, P=0.79) (*Table 2*, *Figure 5*).

The trend of DSCT parameters in rectal tumor progression

The Kendall's tau correlation analysis results demonstrated significant correlations between the DSCT parameters and tumor staging (IC, r=0.709, P<0.001; Zeff, r=0.706, P<0.001; λ, r=0.709, P<0.001; $HU_{40\ keV}$, r=0.704, P<0.001), which suggests DSCT variables correspond to the rectal neoplasm progression to some degree.

Diagnostic accuracy of spectral values in detecting rectal neoplasm

The ROC curves and AUC values of IC, Zeff, λ, and HU_{PEI} for the advanced and early rectal neoplasms are shown on *Figure 6A*,*6B* and *Table 3*, of which DSCT showed a higher ability to detect rectal lesion (P=0.002).

Diagnostic accuracy of spectral values in discriminating the early rectal neoplasm and advanced rectal cancer

The AUC values of IC, Zeff, λ, and HU_{PEI} in discriminating the early rectal neoplasm from advanced rectal cancer were 0.80 (0.73, 0.88; P<0.001), 0.78 (0.71, 0.86; P=0.002), 0.81 (0.74, 0.88; P<0.001), and 0.67 (0.58, 0.75), respectively (*Figure 6C*, *Table 3*). Of note, λ demonstrated the greatest ability in discriminating staging of rectal neoplasm, whereas HU_{PEI} showed the lowest. The optimal cut-off values of IC, Zeff, λ, and HU_{PEI} were 2.05, 8.43, 4.10, and 85.55, respectively. The sensitivities of IC, Zeff, λ, and HU_{PEI} were 0.62, 0.66, 0.64, and 0.51, respectively; whereas the specificities were 0.89, 0.84, 0.89, and 0.76, respectively.

Discussion

Currently, PEI shows high rate of missed superficial and minimal early colorectal neoplasms. In this study, we evaluated the diagnostic value of DSCT in early neoplastic rectal lesions. The present study demonstrates that DSCT has improved ability to detect early rectal cancer and to distinguish early rectal neoplasm from the advanced rectal cancer.

Detection of early rectal cancer from non-endoscopic

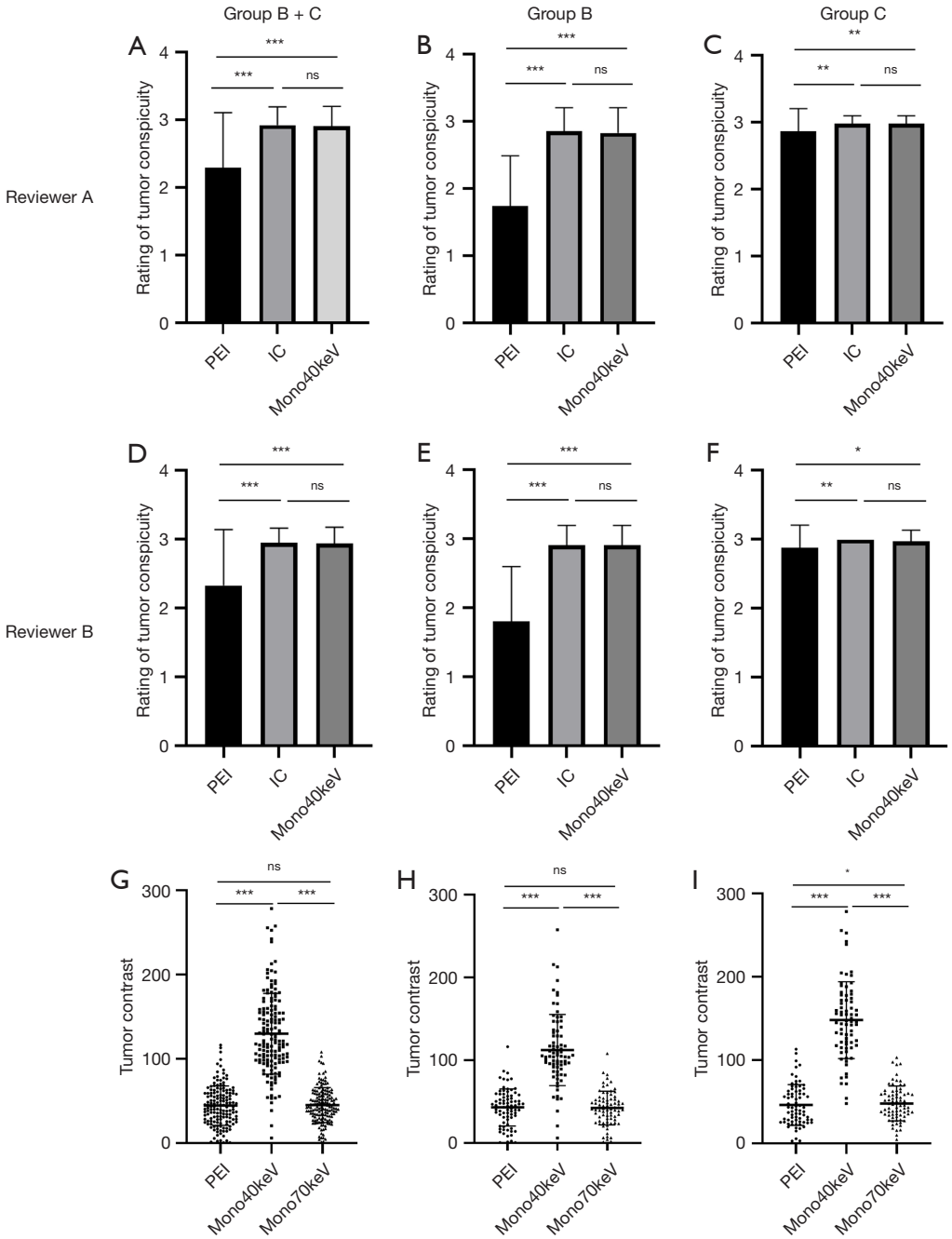

Figure 4 Lesion conspicuity. Bar chart displaying the results of the qualitative reading (A-F). Tumor contrast based on different CT images of all lesions (G), group B (H), and group C (I). ***, P<0.001; **, P<0.01; *, P<0.05; ns, not significant. Group A, the benign group; Group B, the endoscopically-amenable group; Group C, the advanced rectal cancer group. PEI, poly-energetic image; IC, iodine concentration; Mono40keV, mono-energetic images of 40 keV; Mono70keV, mono-energetic images of 70 keV; CT, computed tomography.

examinations has remained an unsolved problem with little useful and effective methods available. Endoscopy is an effective tool to examine the digestive system clearly and thoroughly, but its invasiveness reduces patient acceptance, which can lead to early neoplasms remaining undetected. Contrast-enhanced CT remains the imaging modality of choice of advanced cancer evaluation. However, conventional mixed CT images limit image interpretation

at various energy levels from a single CT examination, negating any potential advantages in early neoplasm detection. DSCT, a multi-parameter imaging mode, acquires a set of virtual monochromatic images of tissues with X-ray at two different energy levels with routine scanning protocol and no more scanning time. DSCT makes it possible to distinguish between materials with different atomic numbers using their energy-dependent attenuation, even if those materials show similar density at PEIs. Besides, post-processing techniques enable further research, including iodine maps, virtual mono-chromatic images, or Zeff images, without increasing radiation dose (16,17). The median dose-length product value of contrast-enhanced abdominal CT for three phases on DSCT was 1,321.00 (1,213.00, 1,460.00) mGy·cm, which is much lower than the Chinese diagnostic reference level (790.00 mGy·cm for one phase). Spectral parameters provide more clinical and function-related information, proving their potential in tumor detection (18), differentiation, and staging (19), extending the capabilities of conventional CT.

Previous research has shown that DSCT can improve tumor staging accuracy for early rectal carcinoma, of which most of the enrolled lesions are of pT2 staging (79.10%, 53/67) (12). To our knowledge, this is the first study to explore the possibility to apply DSCT in detection of early rectal cancer and advanced adenoma. By semiquantitative grading, our results demonstrated that DSCT, especially the images of IC and 40 keV, showed better ability to detect rectal neoplasm especially those superficial and minimal early neoplastic lesions (*Figure 4*), such as advanced adenomas and ≤T1 staging rectal cancer, which have a better prognosis with timely treatment. IC reflects vessel density and blood volume in different tissue regions. Moreover, a high consistency between spectral CT-measured IC and actual IC has been reported. Several studies have shown the performance of quantitative IC measurement in gastric cancer (20,21), hepatocellular carcinoma (22,23), thyroid cancer (24), and other cancer types. Due to the increased angiogenesis during tumor development, the neoplasm was more evident on the iodine maps. Lesions were located on the IC images and the ROC was placed and then copied to other spectral images and PEIs, which made it possible to obtain measurement of PEIs.

Quantitative parameters enable further opportunity to diagnose rectal tumors using DSCT. In our study, there were statistically significant differences in the DSCT-specific parameters among groups, of which $HU_{40\ keV}$, $HU_{70\ keV}$, IC, Zeff, and λ values were significantly higher in advanced rectal cancer than that of early rectal neoplasm and benign bowel wall, and a significant association was

Table 1 Tumor conspicuity based on qualitative reading

Group	PEI	IC	Mono40keV
B+C	3 [2, 3]	3 [3, 3]	3 [3, 3]
B	2 [1, 2]	3 [3, 3]	3 [3, 3]
C	3 [3, 3]	3 [3, 3]	3 [3, 3]

Data are presented as median [interquartile range]. Group B, the endoscopically-amenable group; Group C, the advanced rectal cancer group. PEI, poly energy images; IC, iodine concentration; Mono40keV, mono-energetic images of 40 keV.

Table 2 Comparison of CT assessment

Variable	Group				
	A (n=76)	$B_{bowel\ wall}$ (n=77)	B_{tumor} (n=77)	$C_{bowel\ wall}$ (n=74)	C_{tumor} (n=74)
$HU_{40\ keV}$	100.28±16.24	95.63±18.01	208.01±43.60	107.49±16.96	255.53±45.16
$HU_{70\ keV}$	49.83±10.61	45.13±11.15	87.06±18.55	52.78±11.27	100.78±18.26
HU_{PEI}	51.85 (42.85, 57.95)	44.50±13.99	86.68±19.87	53.70±13.64	99.73±20.53
Iodine concentration (IC, mg/mL)	0.85 (0.73, 0.99)	0.84±0.18	1.91 (1.71, 2.28)	0.95 (0.79, 1.02)	2.58±0.49
Effective atomic number (Zeff)	7.80±0.10	7.80±0.12	8.33 (8.25, 8.50)	7.84±0.11	8.61±0.20
λ	1.69 (1.41, 1.95)	1.68±0.38	3.80 (3.41, 4.52)	1.82±0.36	5.16±1.00

Data are presented as mean ± standard deviation or median (interquartile range) based on the normality. Group A, the benign group; Group $B_{bowel\ wall}$, the normal bowel wall of the endoscopically-amenable group; Group B_{tumor}, the lesion of the endoscopically-amenable group; Group $C_{bowel\ wall}$, the normal bowel wall of the advanced rectal cancer group; C_{tumor}, the lesion of the advanced rectal cancer group. CT, computed tomography; HU, Hounsfield unit; IC, iodine concentration; Zeff, effective atomic number; λ, the slope of the spectral curve.

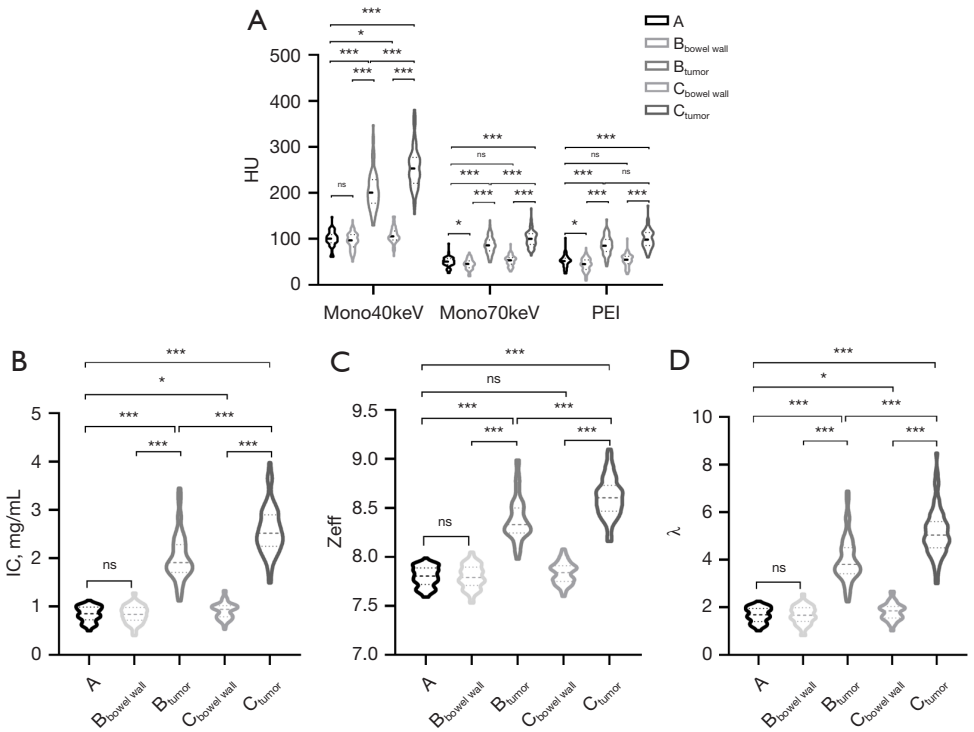

Figure 5 Differences in HU40 keV, HU70 keV and HUPEI (A), IC (B), Zeff (C), λ (D) among groups. ***, P<0.001; *, P<0.05; ns, not significant. HU, Hounsfield unit; Mono40keV, mono-energetic images of 40 keV; Mono70keV, mono-energetic images of 70 keV; PEI, poly-energetic image; IC, iodine concentration; Zeff, effective atomic number; λ, the slope of spectral curve.

found between the spectral parameters and the tumor progression, which can be explained by the differences in tumor angiogenesis. Although the results of mono70keV images show a similar pattern to that of PEIs, they are not the same, since PEIs are of mixed energy. With quantitative measurement, DSCT has highly advantages in detecting early rectal neoplastic lesions.

Our study had several limitations. First, although prospective, this investigation reflects our preliminary experience of DSCT on early rectal tumors with a small number of patients. More clinical trials should be carried out to validate our results. Second, due to the limited number of cases, we did not differentiate patients with advanced adenoma from those with ≤T1 rectal cancer; it is difficult to distinguish them on CT and both could be ideally treated by endoscopic resection. Detailed evaluation can be implemented under endoscopic examination. Third, we set rectal cancer as the object of our study since the rectum is only of 15 cm long, making it easy to identify. Further investigation could be made on other locations of the gastrointestinal tract, such as the esophagus and stomach, to fully explore the potential of DSCT. Fourth, the agreement between readers on rectal tumor conspicuity was low in our study. Since a 3-point Likert scale was applied, it was not easy to assess the early rectal neoplasm accurately, especially on the PEIs, which might be rated as nondiagnostic due to blurring lesions, Grade 2, in most cases, leading to the low agreement between two readers. Moreover, although the performance of the PEIs was comparable to the spectral assessment, the ROIs of PEIs were generated and copied from the IC images. The inevitable selection bias inflates the outcome of the conventional CT, which could be indirectly reflected by its lower lesion detection rate and tumor contrast. PEIs are more likely to miss or misdiagnose in clinical practice. Lastly, even though multiple DSCT parameters were generated from the single scan, individual parameters were used separately for evaluation in our study. Further study is needed to evaluate the potential of multiple parameters to improve the diagnostic power.

In conclusion, DSCT can be used to detect rectal neoplasm, especially the early ones with enhanced image quality. Spectral imaging parameters allow for the detection and differentiation of neoplastic lesions in the rectum,

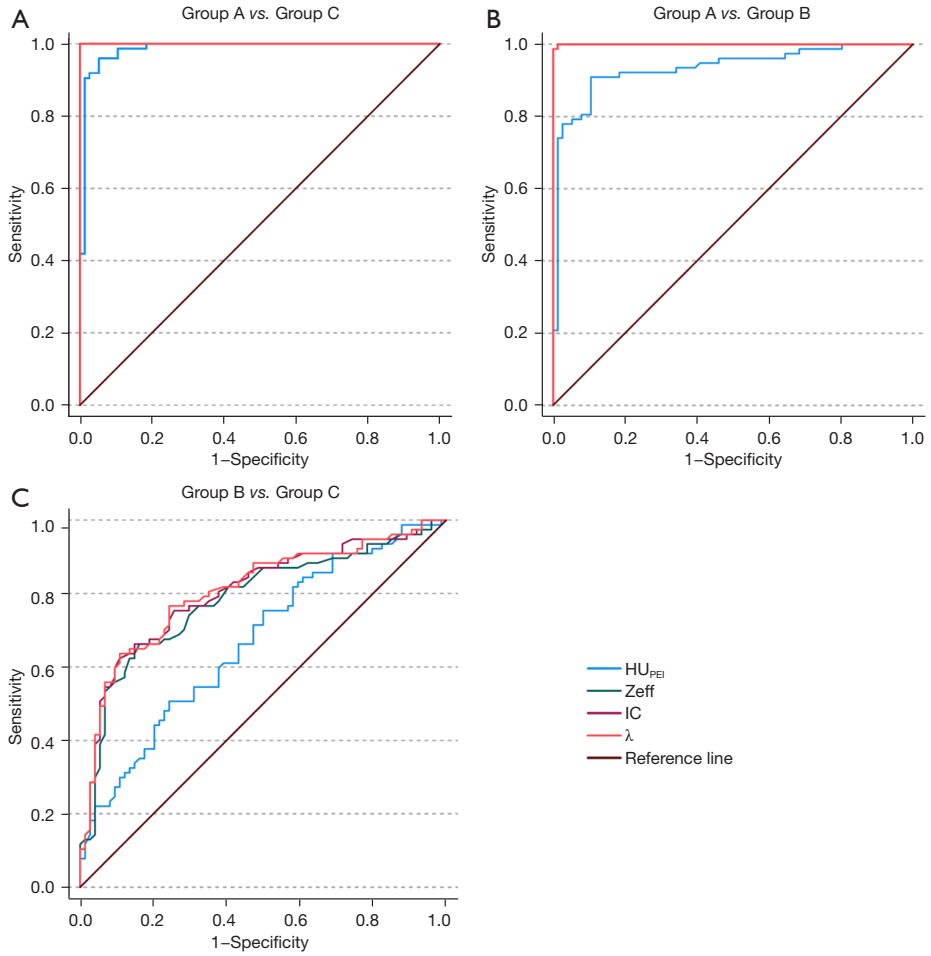

Figure 6 ROC curves for IC, Zeff, λ, and PEI. The ROC curves between advanced rectal cancer and benign rectal wall group (A), early rectal neoplasms and benign rectal wall group (B), and early rectal neoplasm and advanced rectal cancer (C). Spectral parameters have higher AUC value than the conventional one of which ROIs were copied from IC images. Group A, the benign group; Group B, the endoscopically-amenable group; Group C, the advanced rectal cancer group. HU, Hounsfield unit; Zeff, effective atomic number; IC, iodine concentration; λ, the slope of spectral curve; ROC, receiver operating characteristic; AUC, area under the curve; ROI, region of interest.

Table 3 The ROC curves of spectral and poly energetic assessment

ROC	IC	Zeff	λ	HU$_{PEI}$
Group A *vs.* Group C				
AUC (95% CI)	1.00 (1.00–1.00)	1.00 (1.00–1.00)	1.00 (1.00–1.00)	0.99 (0.97–1.00)
Comparison of ROC curves (spectral CT *vs.* PEI), P		0.094		–
Group A *vs.* Group B				
AUC (95% CI)	1.00 (1.00–1.00)	1.00 (1.00–1.00)	1.00 (1.00–1.00)	0.93 (0.89–0.98)
Comparison of ROC curves (spectral CT *vs.* PEI), P		0.002		–
Group B *vs.* Group C				
AUC (95% CI)	0.80 (0.73–0.88)	0.78 (0.71–0.86)	0.81 (0.74–0.88)	0.67 (0.58–0.75)
Comparison of ROC curves (spectral CT *vs.* PEI), P	<0.001	0.002	<0.001	–

Group A, the benign group; Group B, the endoscopically-amenable group; Group C, the advanced rectal cancer group. ROC, receiver operating characteristic; IC, iodine concentration; Zeff, effective atomic number; λ, the slope of the spectral curve; HU, Hounsfield unit; PEI, poly-energetic image; AUC, area under the curve; CI, confidence interval; CT, computed tomography.

which are also highly related to tumor progression.

Acknowledgments

Funding: This work was supported by Chengdu Medical Research Program (No. 2022359 and XZ202301ZY0050G), the National Natural Science Foundation of China (No. 82470536 and No. 82173253), Sichuan Science and Technology Program (22ZDYF1618 and 2022YFH0003), and Undergraduate Teaching Fund of West China School of Medicine (HXBK-B2023052).

Footnote

Reporting Checklist: The authors have completed the STROBE reporting checklist. Available at https://qims.amegroups.com/article/view/10.21037/qims-24-769/rc

Conflicts of Interest: All authors have completed the ICMJE uniform disclosure form (available at https://qims.amegroups.com/article/view/10.21037/qims-24-769/coif). K.D. reports that this study was supported by the funding from Chengdu Medical Research Program (No. 2022359 and XZ202301ZY0050G), the National Natural Science Foundation of China (No. 82470536 and No. 82173253), Sichuan Science and Technology Program (22ZDYF1618 and 2022YFH0003), and Undergraduate Teaching Fund of West China School of Medicine (HXBK-B2023052). The other authors have no conflicts of interest to declare.

Ethical Statement: The authors are accountable for all aspects of the work in ensuring that questions related to the accuracy or integrity of any part of the work are appropriately investigated and resolved. The study was conducted in accordance with the Declaration of Helsinki (as revised in 2013). The study was approved by West China Hospital Institutional Review Board (No. 2024-378) and informed consent was provided by all individual participants.

References

1. Sung H, Ferlay J, Siegel RL, Laversanne M, Soerjomataram I, Jemal A, Bray F. Global Cancer Statistics 2020: GLOBOCAN Estimates of Incidence and Mortality Worldwide for 36 Cancers in 185 Countries. CA Cancer J Clin 2021;71:209-49.
2. Cervantes A, Adam R, Roselló S, Arnold D, Normanno N, Taïeb J, Seligmann J, De Baere T, Osterlund P, Yoshino T, Martinelli E; ESMO Guidelines Committee. Electronic address: clinicalguidelines@esmo. Metastatic colorectal cancer: ESMO Clinical Practice Guideline for diagnosis, treatment and follow-up. Ann Oncol 2023;34:10-32.
3. Brenner H, Heisser T, Cardoso R, Hoffmeister M. Reduction in colorectal cancer incidence by screening endoscopy. Nat Rev Gastroenterol Hepatol 2024;21:125-33.
4. Duffy MJ, Lamerz R, Haglund C, Nicolini A, Kalousová M, Holubec L, Sturgeon C. Tumor markers in colorectal cancer, gastric cancer and gastrointestinal stromal cancers: European group on tumor markers 2014 guidelines update. Int J Cancer 2014;134:2513-22.
5. Bresalier RS, Grady WM, Markowitz SD, Nielsen HJ, Batra SK, Lampe PD. Biomarkers for Early Detection of Colorectal Cancer: The Early Detection Research Network, a Framework for Clinical Translation. Cancer Epidemiol Biomarkers Prev 2020;29:2431-40.
6. Lin JS, Perdue LA, Henrikson NB, Bean SI, Blasi PR. Screening for Colorectal Cancer: Updated Evidence Report and Systematic Review for the US Preventive Services Task Force. JAMA 2021;325:1978-98.
7. Rassouli N, Etesami M, Dhanantwari A, Rajiah P. Detector-based spectral CT with a novel dual-layer technology: principles and applications. Insights Imaging 2017;8:589-98.
8. Chen W, Ye Y, Zhang D, Mao L, Guo L, Zhang H, Du X, Deng W, Liu B, Liu X. Utility of dual-layer spectral-detector CT imaging for predicting pathological tumor stages and histologic grades of colorectal adenocarcinoma. Front Oncol 2022;12:1002592.
9. Li R, Li J, Wang X, Liang P, Gao J. Detection of gastric cancer and its histological type based on iodine concentration in spectral CT. Cancer Imaging 2018;18:42.
10. Sun Q, Bian X, Sun D, Wang M, Dong H, Dai X, Fan G, Zhang L, Li Y, Chen G. The value of preoperative diagnosis of colorectal adenocarcinoma pathological T staging based on dual-layer spectral-detector computed

tomography extracellular volume fraction: a preliminary study. Jpn J Radiol 2024;42:612-21.
11. Peng W, Wan L, Zhao R, Chen S, Dong S, Li L, Zhang H. Novel biomarkers based on dual-energy computed tomography for risk stratification of very early distant metastasis in colorectal cancer after surgery. Quant Imaging Med Surg 2024;14:618-32.
12. Jia Z, Guo L, Yuan W, Dai J, Lu J, Li Z, Du X, Chen W, Liu X. Performance of dual-layer spectrum CT virtual monoenergetic images to assess early rectal adenocarcinoma T-stage: comparison with MR. Insights Imaging 2024;15:11.
13. Giganti F, Dinneen E, Kasivisvanathan V, Haider A, Freeman A, Kirkham A, Punwani S, Emberton M, Shaw G, Moore CM, Allen C. Inter-reader agreement of the PI-QUAL score for prostate MRI quality in the NeuroSAFE PROOF trial. Eur Radiol 2022;32:879-89.
14. Feinstein AR, Cicchetti DV. High agreement but low kappa: I. The problems of two paradoxes. J Clin Epidemiol 1990;43:543-9.
15. Shankar V, Bangdiwala SI. Observer agreement paradoxes in 2x2 tables: comparison of agreement measures. BMC Med Res Methodol 2014;14:100.
16. Matsumoto K, Jinzaki M, Tanami Y, Ueno A, Yamada M, Kuribayashi S. Virtual monochromatic spectral imaging with fast kilovoltage switching: improved image quality as compared with that obtained with conventional 120-kVp CT. Radiology 2011;259:257-62.
17. Silva AC, Morse BG, Hara AK, Paden RG, Hongo N, Pavlicek W. Dual-energy (spectral) CT: applications in abdominal imaging. Radiographics 2011;31:1031-46; discussion 1047-50.
18. Nagayama Y, Tanoue S, Inoue T, Oda S, Nakaura T, Utsunomiya D, Yamashita Y. Dual-layer spectral CT improves image quality of multiphasic pancreas CT in patients with pancreatic ductal adenocarcinoma. Eur Radiol 2020;30:394-403.
19. Li Q, Li X, Li XY, Huo JW, Lv FJ, Luo TY. Spectral CT in Lung Cancer: Usefulness of Iodine Concentration for Evaluation of Tumor Angiogenesis and Prognosis. AJR Am J Roentgenol 2020;215:595-602.
20. Meng X, Ni C, Shen Y, Hu X, Chen X, Li Z, Hu D. Differentiating malignant from benign gastric mucosal lesions with quantitative analysis in dual energy spectral computed tomography: Initial experience. Medicine (Baltimore) 2017;96:e5878.
21. Li J, Xu S, Wang Y, Fang M, Ma F, Xu C, Li H. Spectral CT-based nomogram for preoperative prediction of perineural invasion in locally advanced gastric cancer: a prospective study. Eur Radiol 2023;33:5172-83.
22. Lv P, Lin XZ, Li J, Li W, Chen K. Differentiation of small hepatic hemangioma from small hepatocellular carcinoma: recently introduced spectral CT method. Radiology 2011;259:720-9.
23. Wang Q, Shi G, Qi X, Fan X, Wang L. Quantitative analysis of the dual-energy CT virtual spectral curve for focal liver lesions characterization. Eur J Radiol 2014;83:1759-64.
24. Liu X, Ouyang D, Li H, Zhang R, Lv Y, Yang A, Xie C. Papillary thyroid cancer: dual-energy spectral CT quantitative parameters for preoperative diagnosis of metastasis to the cervical lymph nodes. Radiology 2015;275:167-76.

Cite this article as: Pan X, Wu Z, Zhao J, Zhang X, Zhang X, Tang L, Yang J, Deng K. Early rectal neoplasm in dual-layer spectral detector computed tomography: dual-layer spectral computed tomography (CT) images improve tumor detection and staging. Quant Imaging Med Surg 2024;14(12):8260-8271. doi: 10.21037/qims-24-769